

www.acsami.org Research Article

X-ray Induced Cycling of Rare-Earth Elements between Bulk and Interfacial Liquid

Pan Sun,* Erik A. Binter, Bikash Sapkota, M. Alex Brown, Artem V. Gelis, Mrinal K. Bera, Binhua Lin, Wei Bu,* and Mark L. Schlossman*



Cite This: ACS Appl. Mater. Interfaces 2024, 16, 49935-49943



ACCESS

III Metrics & More

Article Recommendations

s Supporting Information

ABSTRACT: Reversible cycling of rare-earth elements between an aqueous electrolyte solution and its free surface is achieved by X-ray exposure. This exposure alters the competitive equilibrium between lanthanide ions bound to a chelating ligand, diethylenetriamine pentaacetic acid (DTPA), in the bulk solution and to insoluble monolayers of extractant di-hexadecyl phosphoric acid (DHDP) at its surface. Evidence for the exposure-induced temporal variations in the lanthanide surface density is provided by X-ray fluorescence near total reflection measurements. Comparison of results when X-rays are confined to the aqueous surface region to results when X-rays



transmit into the bulk solution suggests the importance of aqueous radiolysis in the adsorption cycle. Amine binding sites in DTPA are identified as a likely target of radiolysis products. The molecules DTPA and DHDP are like those used in the separation of lanthanides from ores and in the reprocessing of nuclear fuel. These results suggest that an external source of X-rays can be used to drive rare-earth element separations. More generally, use of X-rays to controllably dose a liquid interface with lanthanides could trigger a range of interfacial processes, including enhanced metal ion extraction, catalysis, and materials synthesis.

KEYWORDS: rare-earth separations, reversible adsorption, liquid surfaces, interfaces

INTRODUCTION

Ions at liquid interfaces are essential to many processes, including materials development where they influence molecular and particle assembly 1-5 and chemical separations where they determine the efficiency and selectivity of critical element recovery.⁶⁻¹¹ Many of these interfacial processes rely upon neighboring bulk phases as a reservoir of ions. Such processes can be influenced by controlling the properties of the reservoir, such as the concentration of aquo-ions available to be transported to the interface. Control over this transport, from bulk to interface and back, can lead to the triggering of interfacial processes as demonstrated by electrochemical methods for the liquid-liquid interface between two immiscible electrolyte solutions. 12,13 Here, we demonstrate that exposure to X-rays provides control over the cycling of rare earth ions between bulk aqueous solution and its liquidvapor interface.

Rare earth elements are used in many advanced technologies, including permanent magnets, 14 supercapacitors, 15 superconductivity, 16 and sustainable energy systems. 17 Solvent extraction processes to separate and purify rare earth elements from multicomponent aqueous mixtures involve placing the aqueous phase in contact with an organic phase containing amphiphilic extractant molecules that interact with the targeted ions and transport them into the organic phase for further processing. 18,19 Since extractants are believed to complex with ions at the interface, 20 controlling the availability

of ions that can go to the interface can lead to control over the separations process. For example, aqueous complexants are utilized to complex with specific ions in the bulk aqueous phase, preventing them from interacting with extractants and being extracted into the organic phase. A combination of complexants and extractants has been used to advance the separation of actinides and lanthanides, where complexants such as DTPA hold back actinides in the aqueous phase while lanthanides are extracted into the organic phase. 21,22

The competing effects of complexants and extractants contribute to the equilibrium distribution of ions in bulk and interfacial liquids. The concentration and type of complexants and extractants, as well as other factors, including pH, temperature, solvent composition, and reaction and diffusion kinetics are the primary factors used to control solvent extraction processes.^{23,24} Here, we introduce another way to influence the separation of rare earth elements by demonstrating that the equilibrium distribution of rare earth ions can be altered by exposing the bulk liquid to X-rays, thereby

Received: June 14, 2024
Revised: August 10, 2024
Accepted: September 2, 2024
Published: September 10, 2024





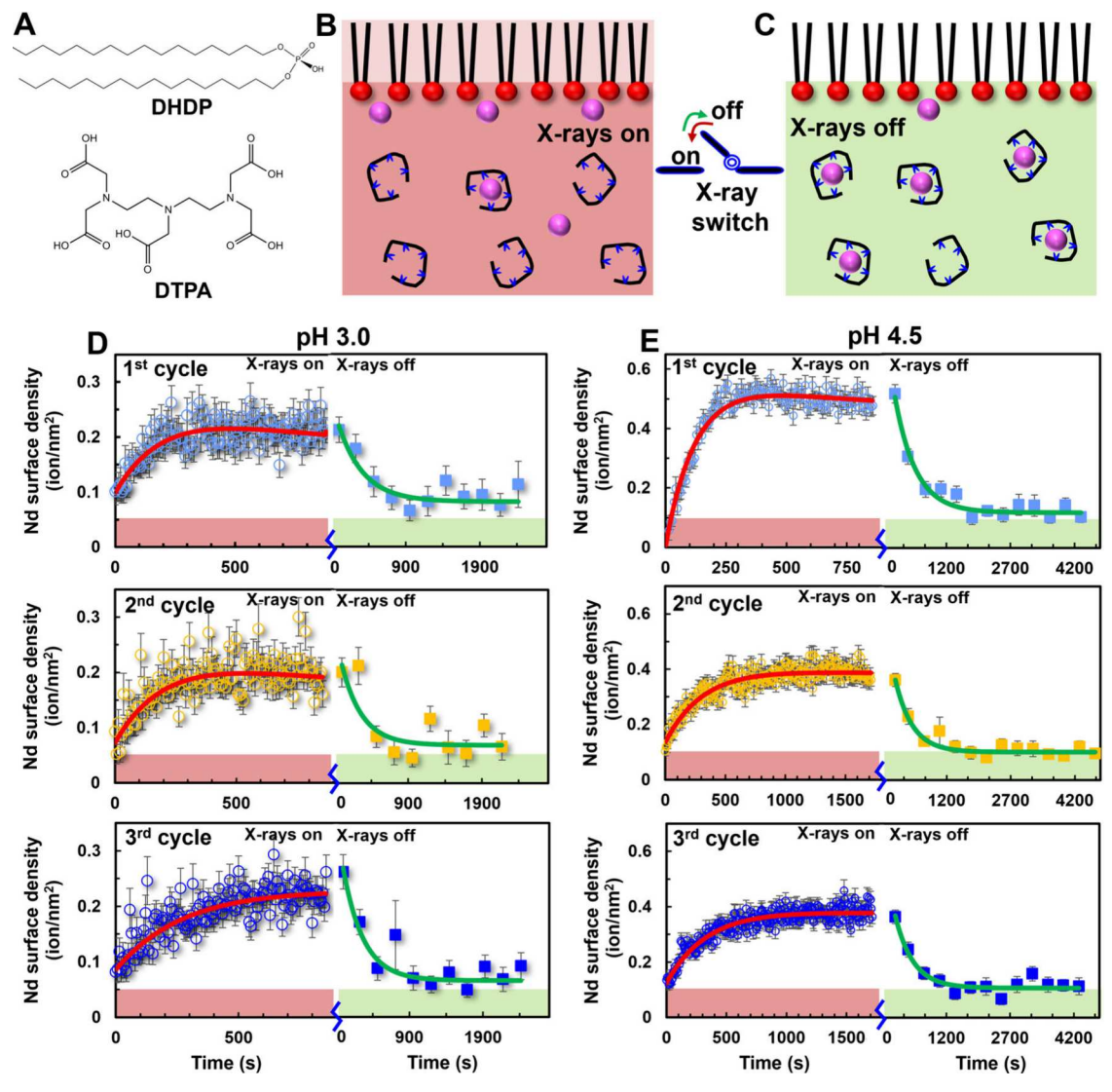


Figure 1. Effect of cycling X-ray exposure on the surface adsorption of Nd^{3+} to a monolayer of DHDP. The monolayer is held at a surface pressure of 10 mN/m on the surface of water containing 30 μ M DTPA, which is a chelating agent, and 10 μ M NdCl₃ (Section S1 for solution preparation). X-ray exposures and measurements were made at the wave vector transfer $Q_z = 0.025 \text{ Å}^{-1}$, which exposes the surface and the bulk aqueous phase within a few micrometers of the surface (Section S2 for X-ray methods). (A) DHDP (dihexadecyl phosphoric acid) and DTPA (diethylenetriamine pentaacetic acid). (B) Illustration of the X-rays-on steady state with a high surface density of ions. Ions are colored magenta, DHDP monolayer at the surface with red phosphoric acid headgroups and black alkyl chains, and DTPA in the bulk (black cages). The red background indicates that X-rays expose the surface and bulk. (C) Illustration of the X-rays-off steady state with a low surface density of ions when most ions are bound to DTPA in the bulk aqueous solution shown in green. (D, E) Temporal evolution of the Nd surface density measured for three cycles at aqueous pH of (D) 3.0 and (E) 4.5. Each cycle consists of an X-ray exposure ("X-rays on") and subsequent recovery ("X-rays off"). X-rays-on refers to continuous exposure of the sample to X-rays with ongoing XFNTR measurements of 5 s duration. X-rays-off refers to a 5-s XFNTR measurement every 5 min without X-ray exposure between measurements. Times marked "0" indicate when the X-rays-on or X-rays-off step started. The color strip at the bottom of each panel also identifies the X-ray exposure (red for on, green for off). Lines are fits described later in the text. Error bars are based upon Poisson statistics of the measurements.

producing a controllable redistribution of ions between the bulk liquid and its liquid—vapor interface.

Our experiments suggest that X-ray radiolysis of the water is likely responsible for the reversible effects reported here. Aqueous radiolysis had been observed previously when water was exposed to the 10 keV X-rays used in this work. The primary molecular and radical products obtained by irradiating water with 10 keV X-rays— H_2 , H_2 O₂, H^{\bullet} , and HO^{\bullet} free radicals, and hydrated electrons—are similar to those produced by irradiation with a variety of higher energy radiation sources such as 60 Co γ -rays. In the context of separations processes, radiolysis products have been implicated

in the reprocessing of nuclear fuel where the radiation source is internal to the solution in the form of ionizing radioisotopes which produce irreversible effects. ^{28,29}

Here, the temporal evolution of the X-ray induced redistribution of ions between bulk liquid and surface is probed by X-ray fluorescence near total reflection (XFNTR), a technique that measures the element-specific surface density of ions at the interface. Short XFNTR measurements of 5 s duration are used to vary the X-ray exposure while measuring the surface density of ions. Carrying out multiple short XFNTR measurements without pausing between them maximizes the total exposure of the sample to X-rays. Infrequent

short XFNTR measurements without X-ray exposure between them are used to minimize the total exposure of the sample, thereby greatly reducing any effects of X-ray exposure, while still allowing for measurements of the ion surface density. A simple model of the surface adsorption kinetics of the ion cycling process is used to summarize the approach to equilibrium of the ion surface density under conditions of ion transport from bulk liquid to interface and back.

In addition, the surface region of the sample can be exposed to X-rays without exposing the bulk liquid by reflecting X-rays from the surface under conditions of total reflection. Larger reflection angles lead to X-ray penetration into the bulk liquid, thereby providing a useful comparison with the surface-only exposure. Experiments on samples with different aqueous pH, as well as different complexants, provide insight into the cycling mechanism. This study demonstrates a method to reversibly control the adsorption of rare earth ions to liquid interfaces.

EXPERIMENTAL METHODS

Materials. Ultrapure water from a Millipore system with resistivity of 18.2 MΩ·cm was used for all aqueous solutions. NdCl₃·6H₂O (99.9%), GdCl₃·6H₂O (99.995%), and chloroform (99.9%) were purchased from Sigma-Aldrich. Dihexadecyl phosphoric acid (DHDP, >98%) was purchased from Avanti Polar Lipids Inc. Sodium hydroxide (NaOH, 98%) was purchased from Alfa-Aesar. Hydrochloric acid (HCl, 36.5 to 38.0%) and trisodium citrate dihydrate (99%) were purchased from Fisher Scientific. Chemicals were used as received without further purification. Solution preparation is described in Section S1 of the Supporting Information.

Langmuir Trough Samples. DHDP monolayers were spread on the surface of aqueous solutions in a Langmuir trough by touching drops of a DHDP-chloroform solution to the surface. Different compositions of the aqueous solutions were chosen as described in the main text. After spreading a dilute submonolayer of DHDP, the trough barrier compressed the DHDP to form a full monolayer. A constant surface pressure of 10 mN/m was maintained with feedback throughout the X-ray measurements. The trough vapor was purged of oxygen for roughly a half hour prior to measurements by flowing helium that had passed through an aqueous bubbler into the trough chamber. The Langmuir trough is a custom design available for use at ChemMatCARS (Sector 15 of the Advanced Photon Source). It has a usable surface area of 120–335 cm² which is much larger than the footprint of the X-ray beam on the water surface (~0.1 cm²) under the conditions of these measurements.

X-ray Exposure. Samples were exposed at ChemMatCARS by reflecting 10 keV X-rays at small incident angles to achieve wave vector transfers of either $Q_z = 0.018 \ \text{\AA}^{-1}$ or $Q_z = 0.025 \ \text{Å}^{-1}$, where $Q_z = (4\pi/\lambda)\sin\theta$ for angle of incidence θ (measured from the plane of the liquid surface) and X-ray wavelength λ . The smaller value of Q_z (= 0.018 Å⁻¹) produces total reflection of X-rays from the sample surface accompanied by an evanescent X-ray wave that penetrates the aqueous solution with a penetration depth of 8 ± 1 nm. The larger value of Q_z (= 0.025 Å⁻¹) produces reflected X-rays and transmitted X-rays, the latter with a penetration depth of of $2.4 \pm 0.1 \ \mu m$ (Section S2 of Supporting Information).

RESULTS AND DISCUSSION

Reversible Cycling of Nd Adsorption. Controlled and reversible adsorption of rare earth neodymium ions to the water-vapor interface was implemented by altering the competitive equilibrium between Nd³⁺ bound to a chelating ligand DTPA dissolved in water and to an insoluble monolayer of DHDP spread on the water surface (Figure 1A). Exposure of the water surface and nearby bulk solution to 10 keV X-rays alters the equilibrium between these two bound complexes,

leading to the reversible transport of ions between surface and bulk liquid as illustrated schematically in Figures 1B and 1C. X-ray exposure unbinds Nd³⁺ ions from DTPA, allowing them to bind to the DHDP monolayer (Figure 1B). Removing the continuous exposure of X-rays allows the DTPA to dominate the binding equilibrium once again and Nd³⁺ ions leave the surface to bind to DTPA in the bulk aqueous phase (Figure 1C).

Evidence for the controlled cycling of Nd³⁺ ions between the bulk and surface of the aqueous solution is shown in Figure 1. Figures 1D and 1E show the temporal evolution of the surface density of Nd during three consecutive cycles of X-ray exposure. Each cycle consists of two steps: X-rays-on and Xrays-off. X-rays-on refers to continuous exposure of the sample to X-rays. During this exposure the element-specific surface density was measured by synchrotron X-ray fluorescence near total reflection (Section S2 for X-ray methods).30 X-ray fluorescence from Nd was generated by X-rays incident on the surface at an angle that is slightly above the angle for total reflection. These X-rays illuminate the surface region and transmit into the bulk aqueous phase with a penetration depth of intensity (normal to the surface) of 2.4 μ m. XFNTR measurements last 5 s each and occur continuously during the X-rays-on exposure. X-rays-off refers to a greatly reduced exposure of the sample for which a 5-s XFNTR measurement occurs once every 5 min but without X-ray exposure between measurements. These experimental results were obtained from samples of a composition and pH for which DTPA is expected to chelate nearly 100% of the Nd3+ ions in solution in the absence of other molecules, such as the DHDP monolayer, or effects such as X-ray exposure (Figure S3B). Figures 1D and 1E show that the surface density of Nd increases during the Xrays-on step and decreases during the X-rays-off step of each cycle. The importance of DTPA and DHDP was demonstrated by control experiments on samples without DTPA and DHDP which revealed a much lower surface density of Nd3+ ions at the surface (0.016 ions per nm², Figure S4).

Effect of X-ray Exposure on DHDP and DTPA. The measurements in Figure 1D/E can be explained as the result of two aspects of X-ray exposure: unbinding of ions from the DHDP monolayer and unbinding of ions from DTPA. As a control experiment, the temporal evolution of the surface density of Nd bound to DHDP at the surface from samples that did not contain DTPA is shown in Figure 2. These measurements demonstrate that the surface density of Nd bound to the DHDP monolayer decreases with time when the sample is continuously exposed to X-rays. It is important to note that other authors have used XFNTR to measure stable surface densities of lanthanide and other ions bound to DHDP monolayers on the surface of water and we also present evidence of stable measurements in the SI (Figure S2).^{20,30} Stable measurements can be obtained by introducing absorber foils into the X-ray beam to reduce the X-ray flux below a critical value. To achieve the measured effects, the measurements in this paper used an X-ray beam flux of 3×10^{10} photons/s which is roughly four times this critical value (Section S2).

The measurements in Figure 2B were taken under similar conditions as those in Figure 1, however, the measurements in Figure 2A were taken with X-rays reflected at a smaller angle of incidence, one which is below the angle of total reflection. In this case, X-rays are totally reflected from the surface at a wave vector transfer of $Q_z = 0.018 \text{ Å}^{-1}$. As described in the

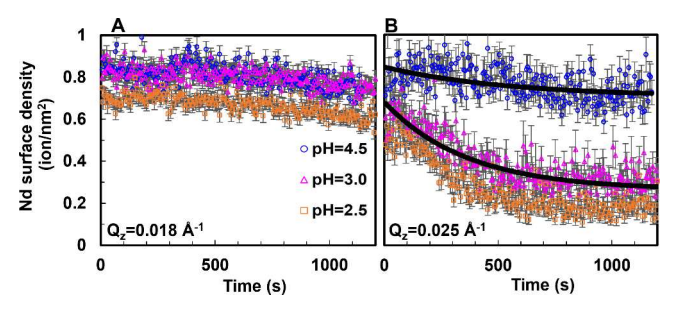


Figure 2. Effect of X-ray exposure on the desorption of Nd from a surface monolayer of DHDP in the absence of DTPA in the bulk liquid. The monolayer was held at a surface pressure of 10 mN/m on the surface of water containing 10 µM NdCl₃. XFNTR measurements of Nd surface density under continuous X-ray exposure with (A) total reflection of X-rays at $Q_z = 0.018 \text{ Å}^{-1}$, which exposes only the surface region, and (B) X-ray reflection at $Q_z = 0.025 \text{ Å}^{-1}$, which exposes the surface and the bulk aqueous phase. Values of pH are 4.5 (blue), 3.0 (magenta), and 2.5 (orange). Two lines in (B) are fits described in the text that are used in a subsequent model of the kinetics for those two values of pH. Error bars are based upon Poisson statistics of the measurements.

Experimental Methods section, total reflection creates an evanescent wave of X-rays whose penetration depth of 8 nm into the water is 280 times smaller than the penetration depth when $Q_z = 0.025 \text{ Å}^{-1}$ (above the angle of total reflection) used for the measurements in Figures 1 and 2B. Greater penetration of X-rays into the water exposes a greater volume of water to X-rays and produces a larger decay of Nd surface density for pH \leq 3.0, as illustrated by comparing Figure 2B to Figure 2A. Since DTPA is not present in the bulk phase of these samples and DHDP is present only at the surface, these results suggest that the interaction of X-rays with bulk water is relevant for the reduction in the surface density of Nd. It is likely that the radiolysis of water by X-rays produces species that interact with the surface monolayer of DHDP to release Nd ions. It is wellknown that aqueous radiolysis produces Ho and HO free radicals, as well as hydrated electrons that react with a wide range of solutes. 28,31-34 The larger effects observed at lower pH in Figure 2B are consistent with previous reports of higher yields of radiolytic species near pH 3 and below in acidic media.²⁷

The XFNTR measurements shown in Figure 2A and Figure 2B were measured from the same sample for a given value of pH, but from different locations on the sample surface. As described in Methods, the size of the X-ray beam spot on the liquid surface was much smaller than the surface of the sample. Measurements in Figure 2A were taken first from one spot of the sample surface, then the beam was moved to another spot for the measurements in Figure 2B, with a time delay of about 2 min. Control experiments showed that the second spot was far enough from the first to be unaffected by direct X-ray exposure of the first spot. The near equivalence of the final values of surface density in Figure 2A to the initial values in Figure 2B shows that the temporal evolution in Figure 2A was due to X-ray exposure that affected the entire sample surface, not just the part of the sample within the X-ray beam spot. These effects were not observed at lower X-ray exposure (Figure S2). Ozone produced by X-rays in the vapor above the sample surface might be responsible for the changes observed in Figure 2A, despite attempts to purge oxygen from the vapor by a helium flow which, however, left roughly 2% oxygen in the vapor above the surface (Section S1).

In the presence of both DTPA in the bulk water and a DHDP monolayer on the water surface, Figure 1D/E shows that the initial measurement in each cycle starts with a low surface density of Nd. For example, the first data point measured for pH 4.5 samples represents a surface density of 0.02 ions nm⁻². It will be shown later that the surface density of Nd remains at this low value for the duration of a long exposure when X-rays illuminate only the surface by reflecting at $Q_z = 0.018 \text{ Å}^{-1}$, for which X-rays are confined to a thin surface region roughly 8 nm thick. This suggests that either direct X-ray exposure of the Nd-DTPA complex in bulk water is required to unbind Nd ions from DTPA, or that radiolysis products from the bulk water interact with the Nd-DTPA complex to release the Nd ions from DTPA. Unbound Nd ions are then free to diffuse to the surface and bind to DHDP which leads to the increase in Nd surface density observed in the Xrays-on part of the cycles shown in Figure 1.

Kinetics Model of Reversible Adsorption Cycling. The total Nd surface density in Figure 1D/E under X-rays-on conditions, $n_{Nd}^{tot,on}$, was modeled by subtracting the Nd ions that desorb from the surface, $n_{Nd}^{des,on}$, from the Nd ions that adsorb to the surface, $n_{Nd}^{ad,on}$,

$$n_{Nd}^{tot,on} = n_{Nd}^{ad,on} - n_{Nd}^{des,on} + b (1)$$

where the constant b represents the initial value of ion surface density for an X-rays-on part of a cycle.

The process of Nd adsorption to the surface likely consists of several subprocesses: release of Nd ions from DTPA dissolved in the aqueous phase, diffusion of Nd ions to the surface, and adsorption to the DHDP monolayer at the surface. Since the experiments do not probe these subprocesses separately, the temporal variation of the surface density $n_{Nd}^{ad,on}$ is approximated by an exponential function,

$$n_{Nd}^{ad,on} = a(1 - e^{-k_1 t}) (2)$$

where the constant a represents the increase in ion surface density due to X-ray exposure that would occur from t = 0 to ∞ , and k_1 is an inverse time constant of the process.

The desorption process detected by XFNTR measurements also includes subprocesses: unbinding of Nd ions from the DHDP monolayer due to X-ray exposure and diffusion of ions out of the surface region. The desorption process is modeled for pH 3.0 and pH 4.5 samples by fitting the data in Figure 2B, which was measured in the absence of DTPA, to an exponential decay, $ce^{-k_2t} + d$. The amplitude c and constant k_2 were determined separately for the different pH values, then used to parametrize the surface density $n_{Nd}^{des,on}$,

$$n_{Nd}^{des,on} = c(1 - e^{-k_2 t}) (3)$$

where the constant c represents the decrease in ion surface density due to X-ray exposure that would occur from t = 0 to ∞ , and k_2 is an inverse time constant of the process.

Substituting eqs 2 and (3) into eq 1 yields the expression used to fit the surface density data in Figure 1D/E measured under X-rays-on conditions,

$$n_{NJ}^{tot,on} = a(1 - e^{-k_1 t}) + b - c(1 - e^{-k_2 t})$$
(4)

Values of c and k_2 were fit to the data in Figure 2B, then used to fit a, b, and k_1 to the X-rays-on data in Figure 1, separately for each pH and cycle. Note that the sum a + b - c is the steady state value if $t \to \infty$ under X-rays-on conditions.

Table 1. Parameters from equations 3 and (4) used to fit the data in Figure 1, where k_2 and c are taken from fits to the data shown by the lines in Figure 2B

	pH 3.0				pH 4.5			
X-rays on	$k_1 (10^{-3} \text{ s}^{-1})$	k_1^{-1} (s) k_2	$(10^{-3} \text{ s}^{-1})^a$	$a + b - c \text{ (ions/nm}^2\text{)}$	$k_1 (10^{-3} \text{ s}^{-1})$	k_1^{-1} (s)	$k_2 (10^{-3} \text{ s}^{-1})^a$	$a + b - c \text{ (ions/nm}^2\text{)}$
1st cycle	$3.8_{0.5}^{0.4}$	260_{30}^{30}	$2.8_{0.6}^{0.6}$	$0.18_{0.05}^{0.03}$	$7.9_{0.5}^{0.6}$	126_8^9	$1.8_{0.6}^{1.0}$	$0.47^{0.04}_{0.04}$
2nd	$3.7_{0.5}^{0.6}$	270_{30}^{40}	$2.8_{0.6}^{0.6}$	$0.17^{0.03}_{0.06}$	$2.8_{0.3}^{0.4}$	353_{41}^{49}	$1.8^{1.0}_{0.6}$	$0.38_{0.05}^{0.05}$
3rd	$3.0_{0.3}^{0.4}$	330_{40}^{50}	$2.8_{0.6}^{0.6}$	$0.23_{0.05}^{0.03}$	$2.6_{0.3}^{0.3}$	379_{41}^{48}	$1.8^{1.0}_{0.6}$	$0.38_{0.05}^{0.05}$
X-rays off	$k_3 (10^{-3} \text{ s}^{-1})$	k_3^{-1} (s)	f (ions/nm	$g ext{ (ions/nm}^2)$	$k_3 (10^{-3} \text{ s}^{-1})$	k_3^{-1} (s)	f (ions/nm ²	$g ext{ (ions/nm}^2)$
1st cycle	$2.9_{0.8}^{1.1}$	34090	$0.14_{0.02}^{0.02}$	$0.08^{0.01}_{0.01}$	$2.0_{0.4}^{0.5}$	490 110	$0.39_{0.04}^{0.04}$	$0.12^{0.01}_{0.01}$
2nd	$3.6^{2.4}_{1.5}$	280_{110}^{190}	$0.15^{0.04}_{0.04}$	$0.07^{0.01}_{0.02}$	$2.5_{0.5}^{0.5}$	400_{70}^{90}	$0.26_{0.03}^{0.02}$	$0.10^{0.01}_{0.01}$
3rd	$3.6^{1.2}_{0.8}$	280_{60}^{90}	$0.20_{0.03}^{0.03}$	$0.07^{0.01}_{0.01}$	$2.4_{0.5}^{0.6}$	420_{90}^{110}	$0.26_{0.03}^{0.03}$	$0.11_{0.01}^{0.01}$

 $a_{k_2}^{-1} = 360_{80}^{120}$ (s) at pH 3.0 and $a_{k_2}^{-1} = 540_{160}^{300}$ at pH 4.5. Superscripts represent a positive error bar and subscripts represent a negative error bar. Error bars on fit parameters are determined by mapping χ^2 space.

The X-rays-off process shown in Figure 1D/E represents the unbinding of Nd ions from the DHDP monolayer, diffusion out of the surface region, and, presumably, binding to DTPA in the bulk water. The total Nd surface density under X-rays-off conditions $n_{Nd}^{tot,off}$ was fit to the data in Figure 1 with an exponential,

$$n_{Nd}^{tot,off} = f e^{-k_3 t} + g ag{5}$$

where f, g, and k_3 are constants determined by fitting and g is the steady state value if $t \to \infty$ under X-rays-off conditions. The fitted parameters to the X-rays-on and X-rays-off data in Figure 1D/E are provided in Table 1.

Interpretation of the inverse time constants k_i in Table 1 is limited by the XFNTR measurements which probe only the surface density of Nd ions. These measurements did not directly probe the subprocesses involved in the addition or removal of Nd ions from the surface. For example, the X-rayinduced release of Nd ions bound to DTPA in the bulk water is not measured directly, Therefore, it is not known whether a direct interaction of X-rays with the bound Nd-DTPA complex released the Nd or whether X-ray radiolysis of the bulk water produced reactive species (such as Ho and HO radicals, and hydrated electrons) which separated Nd from DTPA. Only the indirect effect of increased surface density is observed and the subprocesses of Nd unbinding from DTPA and its diffusion to the surface must be inferred.

The inverse rate constants in Table 1 have values on the order of hundreds of seconds, which likely reveals the diffusive nature of each process in the model. For example, the rate constant k_1 of $n_{Nd}^{ad,on}$ in eq 2 characterizes a process which could involve X-rays producing radiolysis products that diffuse to DTPA, release Nd ions which then diffuse to the surface and bind to DHDP. Alternatively, k_1 could represent the effect of direct release of Nd ions by X-ray exposure but would still involve diffusion of Nd ions from DTPA in the bulk water to bind to DHDP at the surface.

Similarly, the process characterized by the constant k_2 in eq 3 must also contain a diffusive subprocess. As discussed, the measurements of pH 2.5 and pH 3.0 samples shown in Figure 2 suggest that X-ray interactions with the bulk aqueous phase are required. Therefore, the constant k_2 characterizes the time scale to produce radiolysis products in the bulk water including their diffusion to DHDP at the surface to release Nd ions. An exception is that the constant k_2 for pH 4.5 data appears to represent an X-ray exposure process independent of radiolysis effects, as previously discussed. These values of k_2 represent the longest time constants measured.

Finally, the constant k_3 , which characterizes the X-rays-off part of the cycle, represents the equilibration between strongly binding DTPA in bulk water and weaker binding DHDP at the surface when the initial state of the cycle has an excess of ions at the surface. This process also has a long time constant and likely involves either diffusion of DTPA to the surface region or diffusion of Nd from DHDP at the surface to DTPA in the bulk.

An exception to the measured trends shown in Figure 1 is the faster adsorption (k_1) that occurs during the first cycle of pH 4.5 samples, which was also observed when using Gd instead of Nd at this pH (Figure S5). Faster adsorption is accompanied by an initial surface ion density that is small (0.02 ions nm⁻²) compared with the value of 0.1 ions nm⁻² observed at the beginning of subsequent cycles for pH 4.5 samples. We suggest that this effect could be the result of a nonequilibrium initial state of the sample after spreading the DHDP monolayer on the pH 4.5 solution. Although a half hour was allowed for equilibration after spreading for all measurements, this may have been inadequate at pH 4.5. However, a much longer equilibration time was not practical for these synchrotron Xray measurements. In this scenario, X-rays facilitate the release of ions during the initial cycle and subsequent cycling occurs between equilibrium states. Such effects were not observed at pH 3.0.

Steady state values of the ion surface density for the X-rayson part of the cycle, given by a + b - c in Table 1, and the steady state values for the X-rays-off part of the cycle, given by g in Table 1, are larger for pH 4.5 samples than for pH 3.0 samples. This represents the expected enhancement of bound Nd³⁺ over H⁺ to DHDP at higher pH. This is consistent with the measured effective surface pK (= 1.9) of trivalent lanthanum binding to a monolayer of DHDP, as well as known trends in liquid-liquid extraction of lanthanides with a similar extractant, bis(2-ethylhexyl) phosphoric acid (HDEHP).^{36,37} The extraction constant of Nd³⁺ with HDEHP is approximately 15 and the extraction mechanism operates with a third-power H+ dependence in which the equilibrium is shifted to the extracted complex at higher pH. The DTPA and the extractant compete generally between pH 2 and 4 but the distribution of Nd begins to increase past pH 4.5, indicating greater binding to the extractant at higher pH. 37

Irreversibility at Low pH. X-ray exposure-induced adsorption cycles were not observed at lower pH. As an example, Figure 3 shows data measured from pH 2 aqueous samples whose composition is the same as those in Figures 1 and 2. The behavior of the ion surface density in Figure 3A is similar to that observed in Figure 2 for higher pH samples in

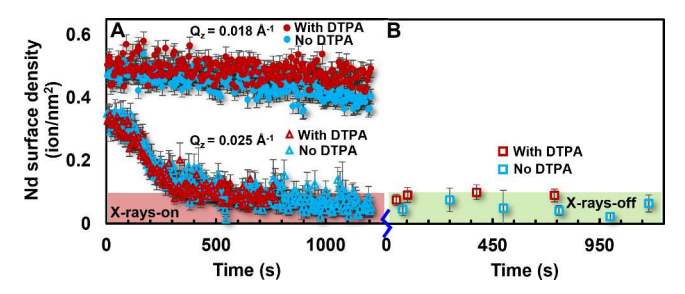


Figure 3. Irreversibility of Nd surface density at pH 2.0. A surface monolayer of DHDP was held at a surface pressure of 10 mN/m on the surface of water at pH 2.0 containing 10 µM NdCl₃ in the presence and absence of 30 μ M DTPA. (A) X-rays-on condition: with (red) and without (blue) DTPA measured at $Q_z = 0.018 \text{ Å}^{-1}$ with surface exposure only (top, dots) and $Q_z = 0.025 \text{ Å}^{-1}$ for which both the surface and bulk are exposed (bottom, triangles). (B) X-rays-off condition: measured at $Q_z = 0.025 \text{ Å}^{-1}$ with (red squares) and without (blue squares) DTPA. The data measured at $Q_z = 0.018 \text{ Å}^{-1}$ and $Q_z = 0.025 \text{ Å}^{-1}$, with and without DTPA, were measured from different samples. Error bars are based upon Poisson statistics of the measurements

the absence of DTPA. In Figure 3A, it is observed that the Nd surface density at low pH is the same in the absence or presence of DTPA. Although it might be expected that the radiolysis effects that released ions from DTPA at higher pH will also do so at lower pH because of the expected increase in radiolysis products at lower pH, 27 it appears that X-ray induced release of Nd ions from DTPA does not affect Nd binding to the DHDP monolayer. At this pH, DTPA is expected to chelate a reduced amount, roughly 40%, of the Nd³⁺ ions in solution in the absence of other molecules or effects (Figure S3B). These measurements suggest that there are enough Nd³⁺ aquo-ions to satisfy the adsorption equilibrium of the DHDP monolayer without the additional release of Nd3+ ions from DTPA by X-ray exposure. As a result of the insensitivity of the ion surface density to DTPA at lower pH values, the net effect of X-ray exposure is ion stripping from the surface, which is the opposite of that observed in Figure 1D/E. Figure 3B shows that the Nd surface density does not recover when X-rays are turned off and an adsorption cycle cannot be established.

Figure 3A also shows that the Nd surface density measured when X-rays are confined to the surface (for $Q_z = 0.018 \text{ Å}^{-1}$) is nearly constant with time. As before, the observation of a temporal variation in the Nd surface density when X-rays penetrate the bulk (for $Q_z = 0.025 \text{ Å}^{-1}$), but not when X-rays are confined to the surface, indicates that aqueous radiolysis products are responsible for stripping Nd ions from the DHDP monolayer. However, the effect is irreversible, which suggests that X-ray exposure at this low pH is damaging the DHDP monolayer. Shifting the X-ray beam to a different position on the sample allows the $Q_z = 0.025 \text{ Å}^{-1}$ data shown in Figure 3 to be reproduced (not shown), confirming that the change in Nd surface density observed at $Q_z = 0.025 \text{ Å}^{-1}$ is not due to changes throughout the entire surface, but is a local effect occurring in the region of the X-ray footprint on the sample. Similar observations for pH 2.25 and pH 2.5 samples are shown in Figures S6 and S7 in the SI.

Considerations on the X-ray Exposure Mechanism. Although the XFNTR technique used in this study cannot identify the molecular reactions that led to the release of Nd ions from either DTPA or DHDP under X-ray exposure, additional experiments were done to provide insight into the

mechanisms that underlie the exposure-induced release. One possibility for the release of Nd ions from DTPA or DHDP is that X-ray exposure reduces Nd³⁺ to Nd²⁺, thereby weakening its binding. Although the oxidation state of 3+ for lanthanides, including Nd, is known to be stable under the solution conditions of these experiments,³⁸ it has been demonstrated that exposure to an ultrahigh pressure mercury lamp can reduce the oxidation state to 2+.39 The authors were successful in synthesizing insoluble Nd(II), Sm(II), and Eu(II) sulfates but were unable to produce Gd(II), citing its lower reduction potential. Nevertheless, if reduction to 2+ was the root cause of these X-ray induced results, the adsorption cycling observed for Nd(III) would not be expected to occur readily for Gd(III) due to its stable half-filled 4f-shell. 40 Therefore, samples containing GdCl₃ substituted for NdCl₃ were used to test the role of lanthanide reduction in the observed X-ray effects. Measurements on pH 4.5 samples containing Gd3+ demonstrated a similar cyclical process as those observed with Nd3+ (Figure S5), indicating that reduction of the lanthanide ion is not required for the X-ray exposure-induced adsorption cycle demonstrated by the data in Figure 1.

Protonation of the amine groups of DTPA would also weaken the binding of Nd³⁺, however, protonation is unlikely to occur at the pH values of the samples because the values of pK_a for the three N groups of DTPA are 6, 7, and 8.⁴¹ However, it has been shown that radiolysis products can cleave N–C and other bonds in ethylamine, triethylamine, and a diamide phenanthroline extractant. 28,31,32 It has also been reported that hydrated electrons and HO radicals can degrade, as well as induce the release of lanthanide and other ions from EDTA (ethylene diamine tetraacetic acid), which is an aminopoly(carboxylic acid) complexant similar in structure to DTPA.33,34 A comparable attack of DTPA by aqueous radiolysis products would result in a loss of the coordination ability of the complexant to lanthanides.

The role of the N-C bond in the observed cycling was tested by substituting trisodium citrate for DTPA. This substitution eliminates nitrogen atoms from the chelate backbone and reduces the number of carboxyl groups from five to three. Both changes reduce the interaction of citrate with Nd3+.42 To compensate for this reduced interaction and create a sample containing citrate whose behavior can be compared with samples containing DTPA, the composition of citrate was chosen to be 10 mM at pH 6. Figure 4C shows that this composition yields a low surface density of Nd ions (0.02 ions nm⁻²) when XFNTR is measured at $Q_z = 0.018 \text{ Å}^{-1}$, for which X-rays illuminate only the surface. This demonstrates that Nd ions are nearly fully chelated by the citrate in bulk water under these conditions, like the nearly full chelation of Nd ions by DTPA demonstrated by XFNTR measured at $Q_z =$ 0.018 Å⁻¹ in Figure 4A (which also revealed a similar surface density of 0.02 ions nm⁻²). A series of results for different pH values varying from 4.5 to 7.5, illustrated in Figure S8, demonstrated that pH 6 at 10 mM provides a condition for which citrate just begins to nearly fully chelate Nd ions. Although it is likely that the composition of the DTPA samples (30 μ M DTPA and pH 3.0 or 4.5) provides a slightly stronger chelation of Nd (compare Figures S3 and S9), the conditions chosen for citrate chelation should be at least equivalently susceptible, if not more so, to the release of Nd when X-rays expose the bulk water. Nevertheless, XFNTR measurements at $Q_z = 0.025 \text{ Å}^{-1}$, for which X-rays illuminate both the surface and the bulk water, did not reveal an increase in surface density

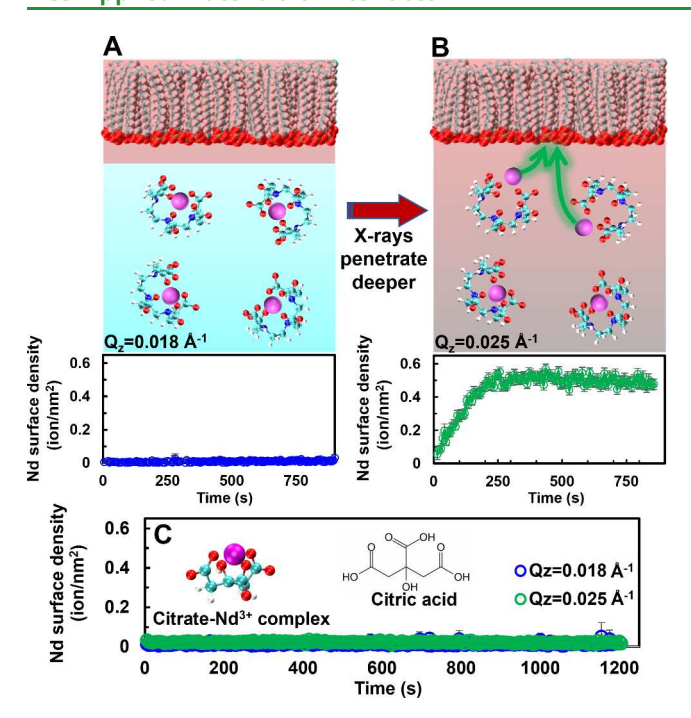


Figure 4. A comparison of citrate and DTPA chelation of Nd ions. Aqueous solutions measured in (A) and (B) contain 10 µM NdCl₃ and 30 μ M DTPA at pH 4.5 with a DHDP monolayer spread at the surface and held at a surface pressure of 10 mN/m. (A) Nd surface density under X-ray illumination at $Q_z = 0.018 \text{ Å}^{-1}$, which confines Xrays to an evanescent wave with an 8 nm penetration depth. (B) Nd surface density under X-ray illumination at $Q_z = 0.025 \text{ Å}^{-1}$, for which X-rays transmit several micrometers into the bulk water. (C) Nd surface density of an aqueous solution containing 10 µM NdCl₃ and 10 mM trisodium citrate (Na₃C₆H₅O₇) at pH 6.0 with a DHDP monolayer spread at the surface and held at a surface pressure of 10 mN/m. Measurements at $Q_z = 0.018 \text{ Å}^{-1}$ (blue) and $Q_z = 0.025 \text{ Å}^{-1}$ (green) overlap each other in contrast to the measurements in (A) and (B). Error bars are based upon Poisson statistics of the

of Nd (Figure 4C) in the presence of citrate, as observed for DTPA samples (shown in Figure 4B and Figure 1). This shows that X-ray exposure will not release Nd3+ from its complexation with citrate, as it does for DTPA. Given the chemical structural similarities of citrate and DTPA, except for the absence of N-C bonds in citrate, these results suggest that the N-C bond in the backbone of DTPA is relevant for the mechanism of X-ray exposure-induced release of Nd3+ ions.

CONCLUSIONS

Reversible cycling of Nd ion adsorption to the surface of an aqueous solution was implemented by using X-ray exposure to alter the equilibrium between Nd bound to DTPA dissolved in bulk water and Nd bound to a monolayer of DHDP on the surface of the aqueous solution. A similar cycling was observed for Gd ions and shown in the SI. A simple model described the measured temporal variation of ion surface density for X-rayson and X-rays-off conditions. The derived kinetic rates correspond to time scales on the order of hundreds of seconds. We suggest that these long processes are most likely dominated by diffusion effects of either ions, radiolysis products, or DTPA, because other processes are expected to be much faster.

Two different modes of X-ray exposure were utilized. When X-rays were reflected below the critical angle for total

reflection, the X-ray exposure was confined to a thin surface region roughly 8 nm thick. Reflection angles above this critical angle led to transmission of X-rays into the bulk aqueous phase for which a much greater number of water and DTPA molecules were exposed. Adsorption cycling occurred only when the bulk liquid was exposed to X-rays. Comparison of the two modes of X-ray exposure allowed us to show the importance of irradiating the bulk liquid for the processes that underlie the cycling of ion adsorption. For example, X-ray exposure effects which reduced the binding of Nd3+ to the DHDP monolayer at pH 3.0 relied upon X-ray exposure of bulk water, which suggested the importance of radiolysis products in the unbinding of Nd3+ from DHDP. X-ray exposure effects which reduced the binding of Nd3+ to DTPA were due either to the radiolysis of bulk water or to direct exposure of DTPA, Although XFNTR measurements could not distinguish between these two mechanisms, the known degradation of aminopoly(carboxylic acid)s by hydroxyl radicals and the much higher concentration of water compared to DTPA suggests that radiolysis of water was responsible.34

Additional experiments provided insight into the molecular mechanism of the unbinding of Nd³⁺ upon X-ray exposure. Substitution of Gd ions for Nd ions suggested that reduction of rare earth ions by X-rays is not relevant for this unbinding process. Substitution of citrate for DTPA suggested that the amines in DTPA are involved in this unbinding.

Reversible cycling was observed at pH 3 and 4.5. At lower pH, such as pH 2, the DTPA does not chelate a sufficiently large fraction of ions to deplete the DHDP monolayer of ions. At pH 2, the bound fraction of ions to DHDP equilibrates essentially independently of the presence of DTPA in bulk solution and adsorption cycling does not occur. The pH values quoted in this study were the values of the sample solution in the Langmuir trough. Although it is possible that the pH is modified in the vicinity of the X-ray exposed regions, it would be challenging to measure local changes in pH because the exposed volume of liquid was orders of magnitude smaller than the sample volume in the Langmuir trough used for these studies (Section S1).

The X-ray reflection geometry employed for this study allowed for simultaneous exposure of the sample and measurement of the ion surface density. As a result of the reflection geometry, exposure of the bulk liquid was accompanied by exposure of the liquid surface. However, the observed processes indicate that exposure of the bulk solution alone is likely to create reversible cycling of ion adsorption. In that case, cycling would require only X-ray exposure of the DTPA in the bulk solution. X-ray exposure would release Nd from DTPA which would then bind to DHDP at the surface. Upon turning the X-rays off the Nd would return to the DTPA because of the favored equilibrium binding between the two. In our experiments, X-ray exposure of the DHDP monolayer affected the time evolution of the Nd3+ surface density but does not seem necessary for the basic process of cycling ion adsorption. Although this has not yet been tested, it appears that exposing the bulk alone should cycle ions between bulk liquid and its surface, which could be relevant for some applications.

The X-ray exposure process that produced reversible cycling of ion adsorption to a water-vapor interface could be used to supply ions in controlled doses to either a liquid-vapor or a liquid-liquid interface. Whether or not cycling will occur at a

liquid-liquid interface would depend upon the behavior of the amphiphile (surfactant or extractant) monolayer at the interface. If binding of ions to the amphiphiles leads them to extract ions into the second phase, then reversible cycling will not occur. However, if a surfactant monolayer remains at the interface upon ion binding, then reversible cycling can be expected at the liquid-liquid interface as well. In both cases, an external source of X-rays could be used to controllably dose the interface with lanthanide ions to drive a range of interfacial physicochemical processes, including catalysis, materials synthesis, and the separation of rare earth elements in liquidliquid extraction and industrial processes.

ASSOCIATED CONTENT

Supporting Information

The Supporting Information is available free of charge at https://pubs.acs.org/doi/10.1021/acsami.4c09905.

> One pdf file containing a description of materials, sample preparation, X-ray methods including analysis protocol for short XFNTR measurements, X-ray exposure dose comparison, DTPA speciation calculations, surface density measurements for cycling Gd(III) samples, Nd surface density measurements at lower pH, Nd surface density measurements with trisodium citrate (PDF)

AUTHOR INFORMATION

Corresponding Authors

Pan Sun - Department of Physics, University of Illinois at Chicago, Chicago, Illinois 60607, United States; NSF's ChemMatCARS, Pritzker School of Molecular Engineering, University of Chicago, Chicago, Illinois 60637, United States; o orcid.org/0000-0002-6128-8656; Email: sunp@ ornl.gov

Wei Bu - NSF's ChemMatCARS, Pritzker School of Molecular Engineering, University of Chicago, Chicago, Illinois 60637, United States; oorcid.org/0000-0002-9996-3733; Email: bu@cars.uchicago.edu

Mark L. Schlossman – Department of Physics, University of Illinois at Chicago, Chicago, Illinois 60607, United States; orcid.org/0000-0003-3238-1250; Email: schloss@ uic.edu

Authors

Erik A. Binter - Department of Physics, University of Illinois at Chicago, Chicago, Illinois 60607, United States; orcid.org/0000-0002-0520-3056

Bikash Sapkota - Department of Physics, University of Illinois at Chicago, Chicago, Illinois 60607, United States; orcid.org/0000-0001-8204-9673

M. Alex Brown - Chemical and Fuel Cycle Technologies Division, Argonne National Laboratory, Lemont, Illinois 60439, United States; o orcid.org/0000-0002-6223-561X

Artem V. Gelis - Radiochemistry Program, Department of Chemistry and Biochemistry, University of Nevada, Las Vegas, Nevada 89141, United States; o orcid.org/0000-0002-5487-1472

Mrinal K. Bera - NSF's ChemMatCARS, Pritzker School of Molecular Engineering, University of Chicago, Chicago, Illinois 60637, United States; o orcid.org/0000-0003-0698-5253

Binhua Lin - NSF's ChemMatCARS, Pritzker School of Molecular Engineering, University of Chicago, Chicago,

Illinois 60637, United States; o orcid.org/0000-0001-

Complete contact information is available at: https://pubs.acs.org/10.1021/acsami.4c09905

Author Contributions

P.S., W.B., and M.L.S. initiated the project. P.S., W.B., M.L.S., M.A.B., A.V.G., M.K.B., and B.L. contributed to project design. M.A.B. and A.V.G. devised radiolysis tests and explanations. E.A.B. and B.S. assisted P.S. in X-ray measurements. The manuscript was prepared by M.L.S. and P.S. All authors discussed results and commented on the manuscript.

Safety Statement. No unexpected or unusually high safety hazards were encountered.

The authors declare no competing financial interest.

ACKNOWLEDGMENTS

This research was performed using funding received from the U.S. Department of Energy, Office of Science, Office of Basic Energy Sciences Separations Program under Award Number DE-SC0018200 to MLS and from the National Science Foundation CHE-1834750 to NSF's ChemMatCARS. This material is also based upon work supported by the NNSA Minority Serving Institutions program under Award Number DE-NE0004008 to MLS, AG, and MAB. Use of the Advanced Photon Source, an Office of Science User Facility operated for the U.S. Department of Energy (DOE) Office of Science by Argonne National Laboratory, was supported under Contract No. DE-AC02-06CH11357.

ABBREVIATIONS

DTPA, diethylenetriamine pentaacetic acid; DHDP, dihexadecyl phosphoric acid; XFNTR, X-ray fluorescence near total reflection

REFERENCES

- (1) Lin, L.; Chowdhury, A. U.; Ma, Y.-Z.; Sacci, R. L.; Katsaras, J.; Hong, K.; Collier, C. P.; Carrillo, J.-M. Y.; Doughty, B. Ion Pairing Mediates Molecular Organization across Liquid/Liquid Interfaces. ACS Appl. Mater. Interfaces 2021, 13, 33734-33743.
- (2) Yin, X.; Chen, Q.; Tian, P.; Zhang, P.; Zhang, Z.; Voyles, P. M.; Wang, X. Ionic Layer Epitaxy of Nanometer-Thick Palladium Nanosheets with Enhanced Electrocatalytic Properties. Chem. Mater. **2018**, *30*, 3308–3314.
- (3) Lund, M.; Jungwirth, P.; Woodward, C. E. Ion Specific Protein Assembly and Hydrophobic Surface Forces. Phys. Rev. Lett. 2008, 100. DOI: 10.1103/PhysRevLett.100.258105
- (4) Chai, Y.; Lukito, A.; Jiang, Y.; Ashby, P. D.; Russell, T. P. Fine-Tuning Nanoparticle Packing at Water-Oil Interfaces Using Ionic Strength. Nano Lett. 2017, 17, 6453-6457.
- (5) Scheu, R.; Chen, Y.; de Aguiar, H. B.; Rankin, B. M.; Ben-Amotz, D.; Roke, S. Specific Ion Effects in Amphiphile Hydration and Interface Stabilization. J. Am. Chem. Soc. 2014, 136, 2040-2047.
- (6) Wang, Z.; Huang, L.; Dong, X.; Wu, T.; Qing, Q.; Chen, J.; Lu, Y.; Xu, C. Ion Sieving in Graphene Oxide Membrane Enables Efficient Actinides/Lanthanides Separation. Nat. Commun. 2023, 14, No. 261.
- (7) Xia, X.; Zhou, F.; Xu, J.; Wang, Z.; Lan, J.; Fan, Y.; Wang, Z.; Liu, W.; Chen, J.; Feng, S.; et al. Unexpectedly Efficient Ion Desorption of Graphene-Based Materials. Nat. Commun. 2022, 13, No. 7247.

- (8) Amesh, P.; Venkatesan, K. A.; Suneesh, A. S.; Maheswari, U. Tuning the Ion Exchange Behavior of Cesium and Strontium on Sodium Iron Titanate. Sep. Purif. Technol. 2021, 267, 118678.
- (9) Zheng, S. P.; Huang, L. B.; Sun, Z.; Barboiu, M. Self-Assembled Artificial Ion-Channels toward Natural Selection of Functions. Angew.Chem., Int. Ed. 2021, 60, 566-597.
- (10) Lu, J.; Zhang, H.; Hou, J.; Li, X.; Hu, X.; Hu, Y.; Easton, C. D.; Li, Q.; Sun, C.; Thornton, A. W.; et al. Efficient Metal Ion Sieving in Rectifying Subnanochannels Enabled by Metal-Organic Frameworks. Nat. Mater. 2020, 19, 767-774.
- (11) Jian, M. P.; Qiu, R. S.; Xia, Y.; Lu, J.; Chen, Y.; Gu, Q. F.; Liu, R. P.; Hu, C. Z.; Qu, J. H.; Wang, H. T.; et al. Ultrathin Water-Stable Metal-Organic Framework Membranes for Ion Separation. Science Advances 2020, 6. DOI: 10.1126/sciadv.aay3998
- (12) Gründer, Y.; Ho, H. L. T.; Mosselmans, J. F. W.; Schroeder, S. L. M.; Dryfe, R. A. W. Inhibited and Enhanced Nucleation of Gold Nanoparticles at the Waterl1,2-Dichloroethane Interface. Phys. Chem. Chem. Phys. 2011, 13, 15681-15689.
- (13) Bera, M. K.; Chan, H.; Moyano, D. F.; Yu, H.; Tatur, S.; Amoanu, D.; Bu, W.; Rotello, V. M.; Meron, M.; Kral, P.; et al. Interfacial Localization and Voltage-Tunable Arrays of Charged Nanoparticles. Nano Lett. 2014, 14, 6816-6822.
- (14) Zheng, B. Z.; Fan, J. Y.; Chen, B.; Qin, X.; Wang, J.; Wang, F.; Deng, R. R.; Liu, X. G. Rare-Earth Doping in Nanostructured Inorganic Materials. Chem. Rev. 2022, 122, 5519-5603.
- (15) He, Y.; Zhou, W.; Xu, J. Rare Earth-Based Nanomaterials for Supercapacitors: Preparation, Structure Engineering and Application. ChemSusChem 2022, 15, No. e202200469.
- (16) Peng, F.; Sun, Y.; Pickard, C. J.; Needs, R. J.; Wu, Q.; Ma, Y. Hydrogen Clathrate Structures in Rare Earth Hydrides at High Pressures: Possible Route to Room-Temperature Superconductivity. Phys. Rev. Lett. 2017, 119, No. 107001.
- (17) Hossain, M. K.; Raihan, G. A.; Akbar, M. A.; Kabir Rubel, M. H.; Ahmed, M. H.; Khan, M. I.; Hossain, S.; Sen, S. K.; Jalal, M. I. E.; El-Denglawey, A. Current Applications and Future Potential of Rare Earth Oxides in Sustainable Nuclear, Radiation, and Energy Devices: A Review. ACS Applied Electronic Materials 2022, 4, 3327-3353.
- (18) Tasker, P. A.; Plieger, P. G.; West, L. C. Metal Complexes for Hydrometallurgy and Extraction. In Comprehensive Coordination Chemistry II: From Biology to Nanotechnology; McCleverty, J. A., Meyer, T. J., Eds.; Elsevier: Oxford, UK, 2004; Vol. 9; pp 759-808.
- (19) Huang, X.; Dong, J.; Wang, L.; Feng, Z.; Xue, Q.; Meng, X. Selective Recovery of Rare Earth Elements from Ion-Adsorption Rare Earth Element Ores by Stepwise Extraction with HEH(EHP) and HDEHP. Green Chem. 2017, 19, 1345-1352.
- (20) Sun, P.; Binter, E. A.; Liang, Z.; Brown, M. A.; Gelis, A. V.; Benjamin, I.; Bera, M. K.; Lin, B.; Bu, W.; Schlossman, M. L. Antagonistic Role of Aqueous Complexation in the Solvent Extraction and Separation of Rare Earth Ions. ACS Central Science 2021, 7, 1908-1918.
- (21) Nilsson, M.; Nash, K. L. A Review of the Development and Operational Characteristics of the Talspeak Process. Solvent Extr. Ion Exch. 2007, 25, 665-701.
- (22) Gelis, A. V.; Kozak, P.; Breshears, A. T.; Brown, M. A.; Launiere, C.; Campbell, E. L.; Hall, G. B.; Levitskaia, T. G.; Holfeltz, V. E.; Lumetta, G. J. Closing the Nuclear Fuel Cycle with a Simplified Minor Actinide Lanthanide Separation Process (Alsep) and Additive Manufacturing. Sci. Rep. 2019, 9, 1-11.
- (23) Rydberg, J.; Cox, M.; Musikas, C.; Choppin, G. R. Solvent Extraction Principles and Practice; Marcel Dekker: New York, NY, 2004.
- (24) Higgins, R. F.; Ruoff, K. P.; Kumar, A.; Schelter, E. J. Coordination Chemistry-Driven Approaches to Rare Earth Element Separations. Acc. Chem. Res. 2022, 55, 2616-2627.
- (25) Lefort, M. Radiation Chemistry. Annu. Rev. Phys. Chem. 1958, 9, 123-156.
- (26) Lefort, M. Phénomènes De Réductions Provoqués Par Les Rayonnements Nucléaires Sur Les Solutions Aqueuses De Composés Minéraux. J. Chim. Phys. 1957, 54, 782-788.

- (27) Ferradini, C.; Jay-Gerin, J.-P. The Effect of pH on Water Radiolysis: A Still Open Question — a Minireview. Res. Chem. Intermed. 2000, 26, 549-565.
- (28) Spinks, J. W. T.; Woods, R. J. An Introduction to Radiation Chemistry, 3rd ed.; John Wiley & Sons: New York, 1990.
- (29) Bobrowski, K.; Skotnicki, K.; Szreder, T. Application of Radiation Chemistry to Some Selected Technological Issues Related to the Development of Nuclear Energy. Topics in Current Chemistry 2016, 374, 60.
- (30) Bu, W.; Vaknin, D. X-Ray Fluorescence Spectroscopy from Ions at Charged Vapor/Water Interfaces. J. Appl. Phys. 2009, 105, No. 084911.
- (31) Bibler, N. E. Gamma and Alpha Radiolysis of Aqueous Solutions of Diethylenetriaminepentaacetic Acid. Journal of Inorganic and Nuclear Chemistry 1972, 34, 1417-1425.
- (32) Chen, Y.; Zhang, P.; Yang, X.; Guo, Q.; Weng, H.; Chong, H.; Shi, W.; Lin, M. Radiolysis of Diamide Phenanthroline Extractant: Exploring the Mechanism of Hno₃ Enhancing the Extraction and An/ Ln Separation Performance after Irradiation. Sep. Purif. Technol. 2023, 318, No. 123994.
- (33) Anbar, M.; Meyerstein, D. Effect of Ligands on Reactivity of Metal Cations Towards the Hydrated Electron, Part 1. The Effect of Ethylenediaminetetraacetic Acid. Trans. Faraday Soc. 1969, 65, 1812-
- (34) Vel Leitner, N. K.; Guilbault, I.; Legube, B. Reactivity of OH and e and e from Electron Beam Irradiation of Aqueous Solutions of Edta and Aminopolycarboxylic Acids. Radiat. Phys. Chem. 2003, 67, 41-49.
- (35) Bevington, P. R.; Robinson, D. K. Data Reduction and Error Analysis for the Physical Sciences, 3rd ed.; McGraw Hill: New York, 2003; Chapter 11.
- (36) Wang, W. J.; Park, R. Y.; Meyer, D. H.; Travesset, A.; Vaknin, D. Ionic Specificity in Ph Regulated Charged Interfaces: Fe³⁺ Versus La³⁺. Langmuir **2011**, 27, 11917–11924.
- (37) Kubota, F.; Goto, M.; Nakashio, F. Extraction of Rare Earth Metals with 2-Ethylhexylphosphonic Acid Mono-2-Ethylhexyl Ester in the Presence of Diethyenetriaminepentaacetic Acid in Aqueous Phase. Solv. Extract. Ion Exch. 1993, 11, 437-453.
- (38) Takeno, N. Atlas of Eh-Ph Diagrams Intercomparison of Thermodynamic Databases. In Geological Survey of Japan Open File Report No. 419; National Institute of Advanced Industrial Science and Technology, Research Center for Deep Geological Environments, 2005.
- (39) Tsushima, S.; Nagasaki, S.; Suzuki, A. Separation and Coprecipitation of Lanthanides and Americium by Photolysis. Nuclear Technology 1997, 118, 42-48.
- (40) Bunzli, J.-C. G.; Eliseeva, S. V. Basics of Lanthanide Photophysics. In Lanthanide Luminescence: Photophysical, Analytical and Biological Aspects, Springer Series on Fluorescence; Hanninen, P., Häma, H.,, Eds.; Springer-Verlag: Berlin Heidelberg, 2010; Vol. 7; pp 1 - 46.
- (41) Brown, M. A.; Paulenova, A.; Gelis, A. V. Aqueous Complexation of Thorium(Iv), Uranium(IV), Neptunium(IV), Plutonium(III/IV), and Cerium(III/IV) with DTPA. Inorg. Chem. 2012, 51, 7741-7748.
- (42) Brown, M. A.; Kropf, A. J.; Paulenova, A.; Gelis, A. V. Aqueous Complexation of Citrate with Neodymium(III) and Americium(III): A Study by Potentiometry, Absorption Spectrophotometry, Microcalorimetry, and Xafs. Dalton Transactions 2014, 43, 6446-6454.